# Surface reconstruction and optical absorption changes for Ge nanoclusters grown on chemically oxidized Si(1 0 0) surfaces

2013 Semicond. Sci. Technol. 28 085009

(http://iopscience.iop.org/0268-1242/28/8/085009)

IOP PUBLISHING SEMICONDUCTOR SCIENCE AND TECHNOLOGY

Semicond. Sci. Technol. **28** (2013) 085009 (9pp) doi:10.1088/0268-1242/28/8/085009

# Surface reconstruction and optical absorption changes for Ge nanoclusters grown on chemically oxidized Si(1 0 0) surfaces

**V S Lysenko**[1], **S V Kondratenko**[2], **Y N Kozyrev**[3], **V P Kladko**[1],
**Y V Gomeniuk**[1], **Y Y Melnichuk**[2] **and N B Blanchard**[4]

[1] Institute of Semiconductor Physics, 41 Prospect Nauki, 03028, Kyiv, Ukraine
[2] Taras Shevchenko National University of Kyiv, 64 Volodymyrs'ka St., 01601, Kyiv, Ukraine
[3] O O Chuiko Institute of Surface Chemistry, 17 Generala Naumova St., 03164, Kyiv, Ukraine
[4] Laboratoire de Physique de la Matière Condensée et Nanostructures Université Lyon 1; CNRS, UMR 5586 Domaine Scientifique de la Doua F-69622 Villeurbanne cedex; France

E-mail: kondr@univ.kiev.ua

Received 10 March 2013, in final form 27 April 2013
Published 19 June 2013
Online at stacks.iop.org/SST/28/085009

**Abstract**

Germanium (Ge) nanoclusters are grown by a molecular-beam epitaxy technique on the chemically oxidized Si(1 0 0) surface at 700 °C. X-ray diffraction and photocurrent spectroscopy demonstrate that the nanoclusters have the local structure of body-centred-tetragonal Ge, exhibiting an optical adsorption edge at 0.48 eV at 50 K. Deposition of silicon on the surface with Ge nanoclusters leads to surface reconstruction and formation of polycrystalline diamond-like Si coverage, while nanoclusters' core becomes tetragonal SiGe alloy. The intrinsic absorption edge is shifted to 0.73 eV due to Si–Ge intermixing. Possible mechanisms for nanoclusters growth are discussed.

(Some figures may appear in colour only in the online journal)

## 1. Introduction

Germanium nanoclusters grown on/in silicon or silicon dioxide have been successfully applied in new nanoelectronic, optoelectronic and memory devices due to quantum confinement effect and possibility of integration within Si-based technology [1, 2]. Heterostructures with epitaxial Ge nanoclusters isolated from Si substrate by an ultrathin silicon oxide layer would be practically promising due to their nanoscale size, tunability and high density. The interest in opto-electronic and solar cells application stems from observation of infrared photoluminescence and photoconductivity caused by optical transitions through confined states of Ge nanoislands (NI). Other important applications of Ge on $SiO_2$ structures include CMOS transistors [3] and nanocrystal nonvolatile memory [4, 5].

The technique of Ge nanoisland growth on Si(1 0 0) covered with ultrathin $SiO_2$ layers is widely accepted now [6]. This technique enables the increase in the nanoisland density up to $10^{12}$–$10^{13}$ $cm^{-2}$ due to thermal decomposition of the ultrathin oxide layer and formation of 'defects' at the surface, that are nucleation centres for both epitaxial and non-epitaxial Ge nanoislands with high aspect ratio varying between 0.2 and 0.6 [7, 8]. Moreover, structures with Ge nanoislands grown by this technique do not contain the underlying germanium wetting layer as for the Stranski—Krastanow mode.

Non-epitaxial Ge nanoislands which are separated from the substrate attract special interest due to spatial separation of electron–hole pairs leading to reduction of recombination rate [9]. NI's growth at the silicon surface covered with ultrathin silicon oxide layer is mainly determined by the dynamics of changes of the $SiO_x$ film structure and physical properties during Ge deposition and is principally possible at temperatures below ~400 °C, when the formation of voids in ultrathin $SiO_2$ films is suppressed [10]. Epitaxy at such low temperatures puts some limitations on the crystallinity and structural perfection of the obtained nanoclusters. Increasing of growth temperature up 430 °C allows us to grow epitaxial crystalline NIs on silicon, while silicon oxide is destroyed due to the thermal decomposition effect [7]. The possibility for high temperature growth of crystalline Ge NIs on top of silicon oxide has not been studied in detail. The question under study is what type of structure of Ge nanoclusters is formed after high temperature growth in the presence of a tetragonal silicon oxide film providing a poor epitaxial relationship to the underlying Si (1 0 0) surface.

In this paper, the technique is suggested for the high temperature growth of crystalline Ge nanoclusters on a chemically oxidized Si surface with the initial 2 nm thick oxide layer, which allows creating the dense arrays of nanoclusters with the tetragonal structure. The main feature of the proposed growth technique is preliminary high vacuum annealing of the silicon dioxide film at 800 °C leading to phase separation [11]. For the first time the Ge nanoclusters with the body-centred-tetragonal (bct) crystal lattice, which are the small band gap material with the absorption edge around 0.48 eV, were obtained.

## 2. Experimental details

The Ge nanocluster structures were grown using a molecular beam epitaxy (MBE) technique on boron-doped ($N_a \sim 10^{17}$ cm$^{-3}$) *p*-Si(1 0 0) substrates with the resistivity of 7.5 Ω cm. A pre-epitaxial chemical oxidation of silicon resulted in formation of a 2 nm thick $SiO_2$ layer on the substrate. The surface modifications were monitored *in situ* using the reflection high-energy electron diffraction (RHEED) technique. The Debay rings in the electron diffraction image showed the presence of an amorphous silicon oxide layer. Prior to Ge deposition the oxidized silicon surface was annealed in vacuum ($\sim 10^{-10}$ Pa) at a temperature of about 800 °C for an hour. The diffraction pattern changed, and appearance of clear and bright Kikuchi lines allowed us to conclude, taking into account the film thickness and the annealing temperature, that phase separation and crystallization in the oxide layer had occurred [11]. Therefore, the film can be considered as a silicon suboxide $SiO_x$ ($0 < x < 2$) with silicon rich regions. Then the substrate temperature was lowered to 700–730 °C, and the deposition of germanium was performed, leading to the formation of Ge nanoclusters on top of the $SiO_x$ layer (structure A).

After deposition of Ge nanoclusters, half of the wafer was covered by a mask, and the system was exposed to a weak flow (2–3 × $10^{14}$ cm$^2$ s$^{-1}$) of Si ions. As a result, on the uncovered part of the wafer SiGe nanoclusters were formed due to additional deposition of silicon with a nominal thickness of around 8 monolayers (MLs) (structure B). Finally, a part of the wafer with as-grown Ge nanoclusters was covered by a 25 nm (45 MLs) thick Si layer (structure C).

Different experimental techniques were employed to characterize the size of nanoclusters. Size distribution and surface densities of the nanoclursters were controlled using atomic force microscopy (AFM) by scanning uncovered structures grown under the same conditions. AFM measurements were performed with an NT-MDT Ntegra microscope in semi-contact tapping mode using Si cantilevers with a tip apex radius of ∼10 nm. High-resolution cross-sectional transmission electron microscopy (HRTEM) observations of a local structure of islands and oxide film were performed on a Gemini scanning electron microscope operating at 200 kV.

X-ray diffractograms for the phase analysis were registered with an X'Pert PRO MRD diffractometer in the reflected beam (Cu $K_\alpha$ radiation, $\lambda = 1.5418$ Å) in the range of angles $2\theta = 20°–70°$ with the scanning step of 0.02° and the acquisition time 5–30 s for each point.

Ohmic Au–Si contacts of rectangular shape and dimensions of 4 × 1 mm were welded into epitaxial layers at 370 °C for lateral photoconductivity measurements. The distance between contacts on the sample surface was 5 mm. Current–voltage characteristics of the structures studied were found to be linear in the range from −10V to + 10V at temperatures between 50 and 290 K. Lateral photoconductivity spectra were measured at excitation energies ranging from 0.48 to 1.7 eV under illumination of a 250 W halogen lamp. The corresponding direct photocurrent signal was registered by a standard amplification technique. Spectral dependences were normalized to the constant number of exciting quanta using a nonselective pyroelectric detector.

## 3. Results

### *3.1. Surface morphology of Ge nanoislands*

The atomic force microscopy image in figure 1(*a*) shows that deposition of germanium onto the $SiO_x$ film at 700 °C results in formation of nanoclusters with the hemispherical top surface and the surface density of $\sim 3 \times 10^{11}$ cm$^{-2}$. The base diameter distribution of Ge nanoclusters is approximated by Gaussian function with a maximum at 16 nm and a full width at half maximum of 6 nm. The mean height was about 10 nm. A typical HRTEM image of Ge nanoclusters grown on silicon oxide is shown in figure 2. We can note a 0.6 (height/base) aspect ratio for Ge islands on silicon oxide much larger than typical values 0.1–0.15 for Stranski–Krastanow islands [12]. The Ge nanoclusters have a crystalline structure, but its quality is strongly affected by twin boundaries, which are observed close to voids in the oxide film. However, most of Ge nanocrystals demonstrate perfect crystallization without any defects (figure 2(*b*). The perfect crystal planes for the Si substrate are observed in figure 2 indicating the high quality of the HRTEM images.

After deposition of 8 MLs of Si onto the surface with Ge nanoclusters, the surface morphology changes (figure 1(*b*)): the mean size of the formed SiGe nanoclusters increases and their surface density decreases to $\sim 10^{10}$cm$^{-2}$, i.e. becomes by a factor of 30 less compared to the Ge nanocluster density for the as-deposited structure. The base diameter distribution of SiGe nanoclusters is approximated by Gaussian function with a maximum at 50 nm and an essentially larger full width at half maximum of 24 nm. The base of the formed SiGe nanoclusters is no longer circular after surface reconstruction,

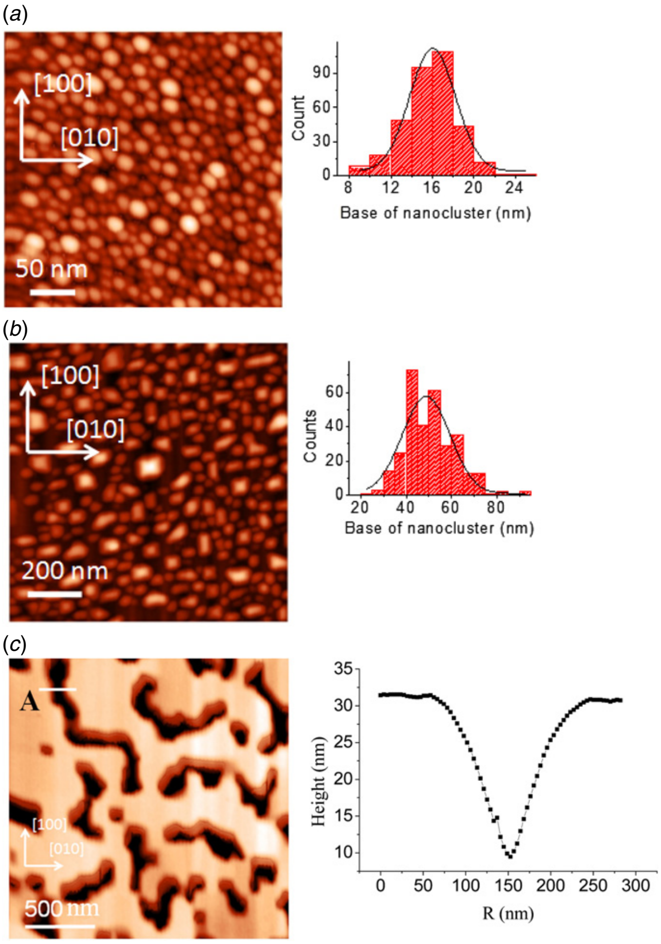

**Figure 1.** (*a*) AFM image of the surface with Ge nanoislands, grown on the surface of $SiO_x$ film and distributions of nanoclusters on base diameters (structure A); (*b*) the same for the surface modified by deposition of 8 Si MLs on the structure with Ge nanoislands (structure B); (*c*) AFM image of the surface of structure C with Ge nanoclusters covered by a 25 nm thick Si layer; (*d*) height distribution along line A.

but becomes polygonal. The average distance between clusters is about 15 nm. Deposition of 45 MLs of Si on the surface with Ge nanoclusters leads to creation of the non-uniform Si layer. The AFM image of structure C with Ge islands covered by a 45 MLs Si layer is shown in figure 1(*c*). The surface of capping Si for this structure contains voids with the depth of about 25 nm.

Additional Si deposition leads to an essential surface reconstruction, so after deposition of 45 Si MLs a nonuniform film was created (see figures 1(*c*) and 4(*b*)) with grooves of 22 ± 1 nm depth and lateral width of 200–400 nm. The profile along the direction A (along the line crossing the void) is presented in figure 1(*c*)). The HRTEM image of the cross-section of the structure is shown in figure 3. The oxide film appeared to vanish after the Si deposition process, and the top layer is crystalline with numerous defects with the maximum density concentrated near the void. Evidently, the bottom of the grooves is the c-Si substrate without Ge nanoclusters. Between the voids the film surface appeared to be smooth, and at the depth of around 20 nm under the surface possibly the interlayer with Ge nanoclusters is present (see figure 3(*b*)).

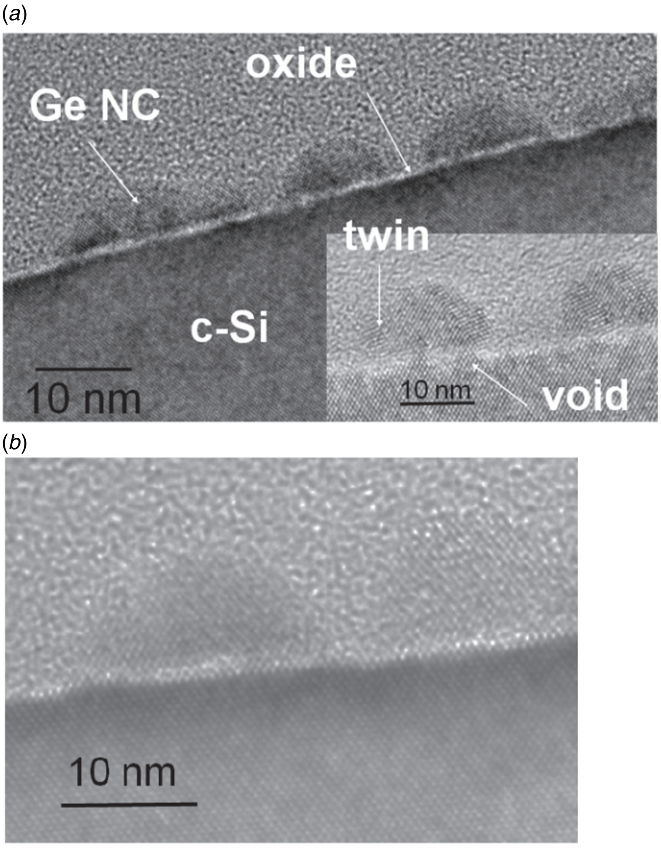

**Figure 2.** (*a*) HRTEM image of Ge nanoclusters on the surface of silicon oxide. Higher magnification images in the inset show the nanoclusters, which contain the twins close to the regions, where they have a contact to the substrate through crystalline voids in the oxide film. (*b*) HRTEM image of crystalline Ge nanoclusters without twins.

Scanning electron microscopy (SEM) images and concentration profiles of Ge, Si and O were recorded using the Auger microprobe JAMP-9500F equipped with an Auger analyzer with the energy resolution $\Delta E/E = 0.05\%$ and using a scanning electron microscope with the resolution in secondary electrons of about 3 nm. SEM images of the structure surface (figure 4) agree with the AFM results.

Figure 5 presents the distribution of concentrations of elements in the near-surface region of the structure with Ge nanoclusters at the surface of silicon oxide (a) and for the same structure but after deposition of 45 Si monolayers (b). Depth profiling was performed by etching of the sample surface by Ar ion beam with the rate of 3.2 nm $min^{-1}$. The depth of the surface layer where the average concentration of elements was registered was ~3 nm. Low concentrations of Ge for sample A proves that the formed nanoclusters are composed of the solid solution $Si_{1-x}Ge_x$. Based on the AFM data, electron microscopy images and concentration profiles, the Ge content in nanoclusters was estimated as ~0.5 ± 0.1. In the structures covered with 45 Si MLs the atomic content of Ge in the near-surface layer was less than 0.5%. Such low concentrations were comparable to the detection limit of the microprobe. As a result, we could only make a conclusion about the presence of Ge, but the precision of the technique did not allow us to determine the concentration profile for this element. The

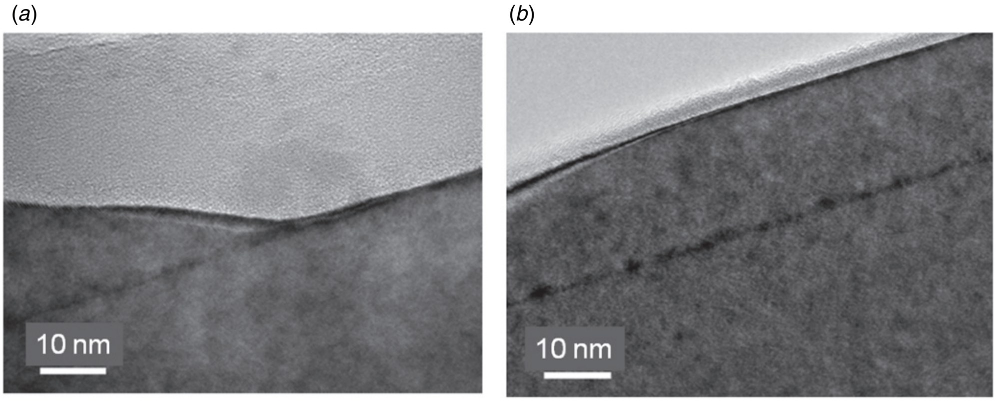

**Figure 3.** HRTEM image of the structure with 45 Si MLs deposited on the surface with Ge nanoclusters.

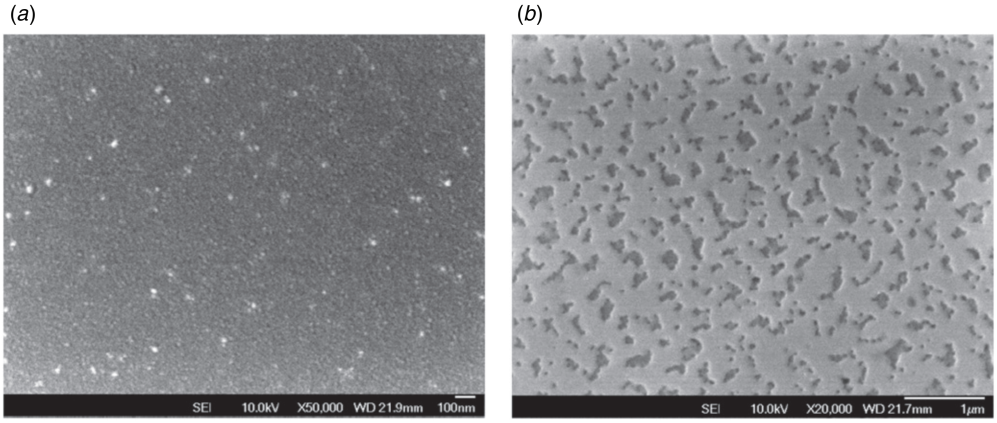

**Figure 4.** SEM image of the surface with Ge nanoclusters grown at the silicon oxide surface (*a*) and of the surface with Ge nanoclusters covered with 45 Si MLs.

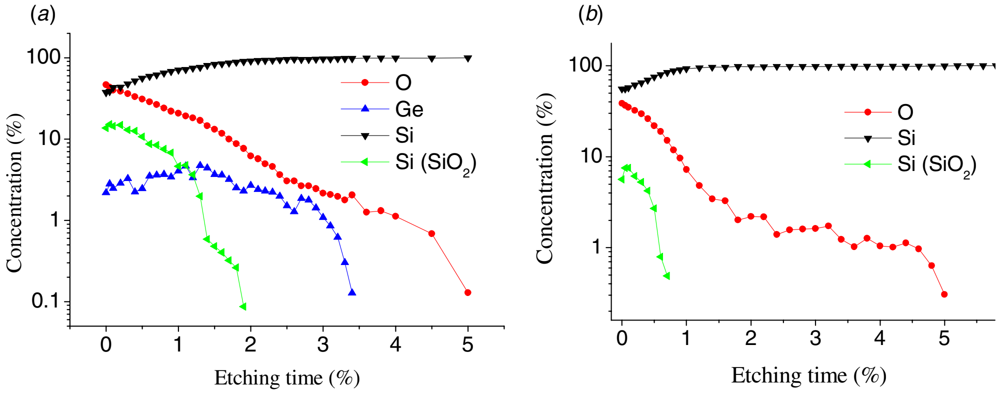

**Figure 5.** Concentration profile of elements in the near-surface region of structures with Ge nanoclusters on the silicon oxide surface (*a*) and for the structure covered with 45 Si MLs (*b*). Etching rate is 3.2 nm min$^{-1}$.

feature of this sample is the high (∼1%) concentration of oxygen in the 15 nm deep surface layer. This reflects the complex mechanism of surface reconstruction and destruction of the oxide layer during Si deposition onto the surface with Ge nanoclusters deposited onto the oxide.

### *3.2. X-ray diffractometry*

Grazing incidence x-ray diffractograms of the studied samples are presented in figure 6 (curves 1–3). The diffractograms were registered at different incident angles of the x-ray beam (XB) in order to detect phases from thin layers. In diffractograms for all the samples, strong reflexes 111 and 200 at various incident angles are observed related to Au (contact material). In the diffractogram of the sample with Ge nanoislands grown on the chemically oxidized Si(1 0 0) surface (curve 1), a weak peak at the angle $2\theta = 24.78°$ was observed at different incident angles of XB. This peak is also present in the diffraction spectra of the structure B with eight monolayers of Si deposited onto the surface with Ge nanoclusters. It can be attributed to the reflex 111 of the tetragonal modification of Ge (ICDD, PDF-2,

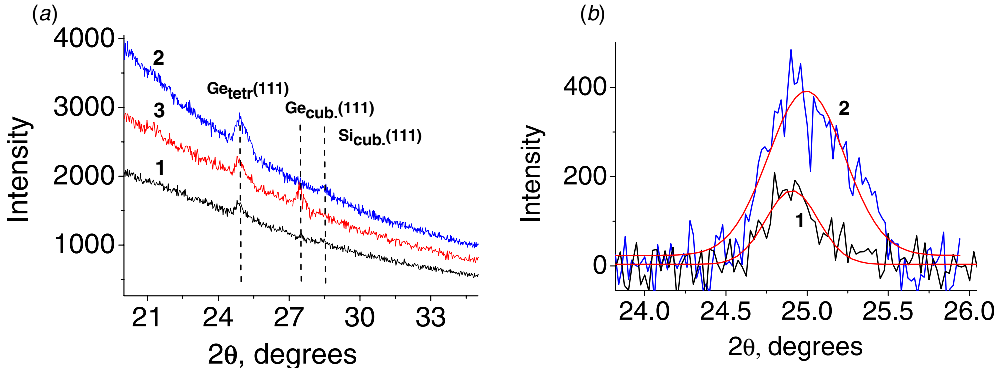

**Figure 6.** (*a*) X-ray diffraction spectra for samples, recorded at incident angle $\omega = 0.5°$. 1—as-grown sample with Ge nanoclusters grown on chemically oxidized Si(1 0 0); 2—covered with 8 MLs of Si; 3—covered by 25 nm thick Si layer. (*b*) Peaks of 111 reflex of tetragonal modification of Ge derived from spectra for the as-grown sample with Ge nanoclusters (curve 1) and the sample with 8 MLs of Si (curve 2).

01-072-1089 (Tetragonal II-Ge: $a = b = 5.9300$ Å, $c = 6.9800$ Å)). In diffraction patterns of the structure with SiGe nanoclusters (sample B) at a grazing incidence of XB, the peak is observed at Bragg angle $2\theta = 28.587°$, close to the the diffraction angle for the cubic phase of silicon (reflex 111). This peak can be attributed to $Si_{1-x}Ge_x$ alloy, which is formed due to intermixing of the Si and Ge atoms during silicon epitaxy onto the surface of Ge nanoclusters [13].

In diffraction spectra of the sample with 45 MLs of Si deposited onto the surface with Ge nanoclusters, the intensity of 111 reflex for the tetragonal Ge phase decreases, and the reflex appears at 27.5°, close to the diffraction angle from the cubic phase of germanium 111 $Ge_{cub}$ (curve 3). The peak at $2\theta = 28.587°$, which was observed for the structure with Ge nanoclusters covered by 8 MLs of Si (curve 2), is not observed for the structure with 45 MLs of Si (curve 3).

Since in the diffraction spectra the reflexes are present for different reflections from clusters and silicon layers both in grazing incidence and $\theta$–$2\theta$ geometries, the conclusion can be drawn that the material of clusters and the epitaxial silicon layer have a polycrystalline structure. However, experimentally we could detect and analyze only a strong reflex 111.

### *3.3. Photocurrent spectra*

To study experimentally optical absorption spectra of the structures with nanoclusters, we used the spectroscopy of lateral photoconductivity [14, 15]. This technique allows studying the spectral features of nano-sized objects, contribution of which into the total light absorption is weak due to small sizes of investigated structures. Spectral dependences of photoconductivity were measured in a wide temperature range from 50 to 290 K. Contribution of non-equilibrium carriers, excited in nanoclusters, increases at lower temperatures. Figure 7 shows the lateral photoconductivity spectra at 50 K for Ge–$SiO_x$–Si heterostructures with Ge nanoclusters at the $SiO_x$ surface (curve 1), for the heterostructure with SiGe nanoclusters (curve 2), and for the structure with Ge nanoclusters covered by 25 nm thick Si layer (curve 3).

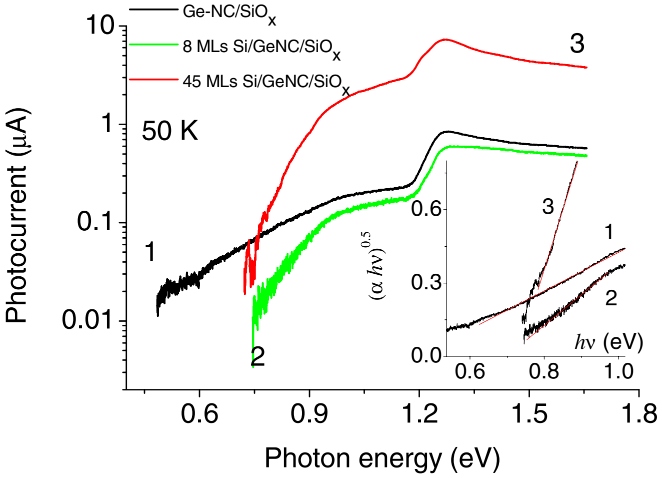

**Figure 7.** Lateral photoconductivity spectra at 50 K for heterostructures with Ge nanoclusters at the $SiO_x$ surface (curve 1), for the structure with Ge nanoclusters modified by Si deposition (curve 2), and for the structure with 25 nm thick Si layer deposited on the top of Ge nanoclusters (curve 3). The inset shows a low-energy fraction of the spectrum plotted in $(\alpha(h\nu)\,\dot{c}\,h\nu))^{0.5}$ versus $h\nu$ coordinates.

In the structure with Ge nanoclusters, the photoconductivity edge was found at quantum energy $h\nu > 0.48$ eV. Deposition of Si onto the surface with Ge nanoclusters leads to the shift of photoconductivity (absorption) spectra towards higher quanta energy (figure 7, curve 2). The long-wavelength edge of photoconductivity spectra was observed at around 0.73 eV. Subsequent deposition of the 25 nm thick Si layer to the surface with Ge nanoislands did not cause a further modification of spectra (figure 7, curve 3) However, in the heterostructure with Ge nanoislands covered by a 25 nm thick Si layer, the photoresponse and the dark conductivity were an order of magnitude higher.

## 4. Discussion

The use of a chemically oxidized Si surface with the initial 2 nm thick $SiO_2$ film allows formation of crystalline Ge nanoclusters, which are separated from the substrate by the thin oxide layer, at high (~700 °C) temperature. One of the key differences of the proposed technique for the formation of Ge nanoclusters is preliminary modification of the chemically oxidized Si(1 0 0) surface. During the high-vacuum annealing of $SiO_2$ film at 800 °C for an hour, the thermal decomposition and desorption of the silicon dioxide film take place according to the reaction

$$SiO_2 + Si \rightarrow 2SiO\ (\text{gas}). \qquad (1)$$

This process takes place at the $SiO_2$/Si interface leading to formation of voids in $SiO_2$ with further lateral widening [15]. Process (1) can be successfully used for Si surface cleaning prior to epitaxial growth. In our case, we stop desorption and decomposition of the oxide film at the initial stage, when the voids have appeared on the top surface only. As a result, the non-stoichiometric $SiO_x$ ($x \leqslant 2$) layer is formed containing nonbridging oxygen hole centres and first oxygen-deficiency centres (E' centres). Two neighboring E' centres can be transformed into the neutral oxygen vacancy, in which two incomplete tetrahedra are linked by Si–Si bond [16]. The Si–Si bonds on top of the oxide film are the nucleation centres for Ge nanocluster formation. During deposition of the first germanium monolayer onto the silicon oxide, the absorption layer is formed, which, starting just from the second monolayer, is transformed into nanoclusters that nucleate randomly on top of chemical $SiO_2$. Such a type of surface reconstruction is energetically favourable in the case if the direct contact with the Si(1 0 0) substrate is poor, i.e. when the oxide layer is still present [17].

The AFM image shows two types of Ge nanoclusters grown on the oxide film. The smallest clusters shown in figure 1(*a*) have circular bases. The large islands (figure 1(*b*)) are oblong in shape having base sides oriented randomly with respect to substrate directions [1 0 0] and [0 1 0]. They are created in the result of coalescence of many smaller islands. Presented images also show examples of two Ge nanoclusters that have just begun coalescence. It is significant to note that the boundaries between merged clusters have different angles in respect to [1 0 0] and [0 1 0] direction of Si substrate. We can suppose that Ge nanoclusters have a poor epitaxial relationship with Si(1 0 0) substrate, i.e. are tilt-misoriented to the underlying Si substrate. The HRTEM image shows the presence of defect-free crystalline Ge nanoclusters, which are separated from Si(1 0 0) by the silicon oxide film with a thickness of 1 nm (figure 2(*b*)). Reduction of oxide thickness from the initial value of 2 nm to 1 nm is due to pre-growth thermal destruction of the silicon dioxide according to reaction (2). Crystalline clusters in silicon oxide beneath Ge nanoclusters start to nucleate during high vacuum annealing of the oxide film at 800 °C, while the $SiO_x$ film is separated into more stable $SiO_2$ and Si clusters. We cannot also exclude that formation of crystalline clusters in silicon oxide continues during Ge growth. The presence of similar localized inclusions in ultrathin silicon oxide film which exhibit single crystalline character has been previously reported [18, 19]. The width of these clusters is 2–3 nm and the surface density is $10^{11}$ cm$^{-2}$, which agrees with the observed density of Ge nanoclusters.

X-ray diffraction spectra show the tetragonal crystalline structure of Ge nanoclusters grown on oxide films, which points to a more complex mechanism of nanoclusters formation, than nucleation on silicon voids described in [18, 19]. The crystalline voids shown in figure 2(*a*) (inset) may also appear under nanoclusters during deposition of Ge. They are centres of defect generation due to effect of Si cubic lattice on the crystal structure of Ge tetragonal nanoclusters, which were nucleated randomly and had no epitaxial relationship to the substrate initially. Twin boundaries are observed in some Ge nanoclusters having direct contacts to Si substrate through crystalline regions (figure 2(*a*), inset). The high density of twin defects has also been observed in Ge films created from nucleation and coalescence of Ge islands within small crystalline openings in $SiO_2$ template in twin relationship to silicon substrate [20]. Twinning of the (1 1 1) planes is also observed for Ge nanoclusters embedded in $SiO_2$, while the distance from islands and Si(1 0 0) substrate is less than 2 nm [11].

In spite of connection to the substrate through crystalline voids in oxide the usual diamond-like crystal structure of Ge appears to be completely absent in nanoclusters grown on the oxide film. When the initial stage of nanoclusters growth on the oxide layer takes place, the epitaxial relationship with the Si(1 0 0) substrate is poor, and Ge nanoclusters with tetragonal structure are created, because the type of their crystal lattice is determined mainly by the local structure of $SiO_x$ film near the sites of nucleation centres generation. In the process of Ge epitaxy, Si–O chemical bonds nearest to the cluster nucleation centres are being broken, which leads to the substitution of oxygen atoms by Ge atoms and to formation of the tetragonal polycrystalline structure. The existence of body-centred-tetragonal phase (Ge II) is secured by compressive deformations, appearing when Ge adatoms are linked to the nanocluster nucleation centres (Si–Si bonds) due to different length of Si–O cristobalite (1.63 Å) and Ge-Ge (2.45 Å) bonds [21, 22]. As described in [21], another possible way for obtaining body-centred-tetragonal phase of germanium (Ge II) is the heteroepitaxial growth on the (1 1 1) surface of a Ge–Sn buffer layer. There are experimental reports of a simple tetragonal structure of Ge nanocrystals [23–25]. In the bulk, the tetragonal Ge phase is only obtained from high-pressure experiments. For example, the semiconducting diamond-structure phase (or Ge I) can be transformed to $\beta$-tin structure (or Ge II) at a hydrostatic pressure of approximately 100 kbar [26]. The reason for long-term tetragonal lattice conservation for Ge nanoclusters is not presently understood.

Epitaxy of Si on the surface of the structure with tetragonal Ge nanoclusters leads to essential modification of the surface topology and morphology. The AFM image, shown in figure 1(*b*) for sample B, indicates a dramatic decrease of the density of nanoclusters. An irregular shape of nanoclusters is due to coalescence intensified by silicon deposition. It can be suggested that at the initial stages of heteroepitaxy Si adatoms are selectively linked only to dangling Ge bonds at the surface of nanoclusters, though at the oxidized silicon surface between the Ge nanoclusters the reaction of thermal decomposition of silicon oxide may take place, according to reaction (1), and the new voids of Si(1 0 0) substrate can also be formed despite the presence of a sufficiently thick oxide layer. Due to the lattice mismatch between Ge and Si, the elastic energy is accumulated in the process of the nanoisland growth. At the same time the distance between bases of adjacent nanoclusters reduces. While reaching the critical magnitude of deformation, the total energy of the system can decrease at the expense of a collapse of spacing between nuclei and due to reduction of the surface energy. Coalescence of nanoclusters occurs when the sum of the elastic energy, generated at the unit area, and of the grain boundary energy is equal to the energy of two free surfaces of separate crystallites. In this case, the tetragonal structure of SiGe nanocrystallites is kept. Their aggregation into nanoclusters is provided by the epitaxy of the linking material—Si. The evidence of the described polycrystallinity is the polygonal base of the formed SiGe nanoclusters (see figure 1(*b*)) and substantial (by a factor of 30) reduction of the surface density of nanoclusters after the surface reconstruction. The smallest clusters have a complicated (polygonal) shape with different orientation of sides. The larger nanoclusters have rectangular base with sides oriented along the [1 0 0] and [0 1 0] directions of underlaying Si(1 0 0), i.e. have an epitaxial relationship to substrate due to decomposition of the oxide layer during coalescence and deposition of silicon. Formation of silicon coverage with high concentration of defects after deposition of Si atoms on the surface with Ge nanoclusters, which leads to continuation of nanoclusters growth with further coalescence, was reported in [17].

As follows from x-ray measurements, SiGe nanoclusters contain tetragonal phase of Ge. It should be mentioned, that at used temperatures of nanocluster growth of about 700 °C the possibility of Si penetration into Ge nanoclusters with formation of $Si_{1-x}Ge_x$ alloy with the tetragonal modification cannot be ruled out. The reflex of the tetragonal germanium phase in diffraction spectra of the structures with Ge nanoclusters was found at 24.9° (see figure 6(*b*)). After Si deposition, the shift of the peak was observed from tetragonal Ge by 0.1° towards greater angles, indicating reduction of the lattice parameter while formation of $Si_{1-x}Ge_x$ alloy with the tetragonal lattice. We associated observed changes in intensity and peak position with creation of SiGe tetragonal alloys due to interdiffusion during deposition of silicon on top of Ge nanoclusters. The bulk of tetragonal polytype becomes larger; therefore, peak area is expected be increased. Moreover, the increase of the peak width for Ge nanoclusters can be related to the gradient of Si content in nanoclusters.

The appearance of the diffraction peak Si (1 1 1) at Bragg angle $2\theta = 28.587°$ indicates that the shell of nanoclusters also appears to be crystalline with a cubic unit cell Si (or $Si_{1-x}Ge_x$ alloy with low Ge content). Thus, silicon at the surface of SiGe nanoclusters does not continue creating a tetragonal lattice. This effect is evidently explained by the fact, that in the case of bct Si lattice formation at the surface of Ge nanoclusters, the lattice mismatch would generate tensile stresses in capping Si. The sign of generated deformations makes the process of creation of cubic Si (or $Si_{1-x}Ge_x$ alloy), instead of its tetragonal modification, more energetically favourable.

After capping of Ge nanoclusters by 45 MLs of Si, the SiGe cubic phase is also formed, possibly, due to reduction of the fraction of the tetragonal phase. The possible reason for this effect is relaxation of elastic stresses in nanoclusters due to Si–Ge intermixing and plastic deformations. Besides, in the process of Si epitaxy, destruction of the oxide layer between adjacent SiGe nanoclusters may take place, which can lead to the possibility of the multiple contacts to Si(1 0 0) substrate, promoting the construction of the cubic lattice.

Removal of $SiO_x$ near the base of nanoclusters during Si deposition leads to generation of strong deformations which promote the surface diffusion of Ge atoms from the nanoclusters to the freshly exposed Si surface around the islands. As was pointed out in [20], the magnitude of the stresses is higher for nanoclusters with better epitaxial relationship; therefore, such clusters will be dissolved more effectively. As a result, the nanoclusters with different epitaxial relationship to the substrate will be dissolved with different rates in the oxide film in the process of its destruction, leading to creation at these places of non-uniform SiGe wetting layer with high concentration of silicon. In favour of this assumption, we can suggest the following arguments. First, HRTEM images of sample B did not contain twins, indicating the full dissolution of nanoclusters, in which they were observed. Second, a partial dissolution of many nanoclusters in the process of Si deposition is confirmed by the results of Auger analysis which shows an essential reduction of Ge content in structure C compared to the sample with non-covered Ge nanoclusters (see figure 5). On the other hand, the peak in the diffraction spectra that corresponded to the tetragonal Ge (or SiGe) phase was still observed after Si deposition. This can mean that misoriented tetragonal Ge nanoclusters which have a poor relation to the Si substrate and do not contain twins, are stable against dissolution.

New crystalline voids and nondissolved clusters on the surface of oxide films are the source of numerous defects and crystalline structure disorder of capping Si. The AFM image of sample C shows discontinuous Si film containing 25 nm deep voids, and confirms strong influence of defects on its formation. Apparently, disappearance of diffraction peak Si(1 1 1) at Bragg angle $2\theta = 28.587°$ for structure C, in contrast to the results observed for structure B, indicates the disordered structure of Si cover layer. After deposition of 45 ML Si coverage the silicon oxide film is completely destroyed in the region between Ge NCs. Therefore, the created Si epilayer has an epitaxial relationship with Si (1 0 0) substrate due to numerous connections. Created polycrystalline Si(1 0 0) coverage with cubic lattice as well as Si(1 0 0) substrate cannot contribute to XRD spectra measured in grazing incidence geometry. Under these conditions the tetragonal phase of nanoclusters is essentially affected by the cubic lattice of the silicon epilayer and silicon substrate. As a consequence, in structure C with 45 MLs of Si in the diffraction pattern the reflex of the cubic germanium phase appears, which was absent in the structure with eight deposited Si MLs.

Measurements of infrared photoconductivity confirmed the above suggestions about the structure of nanoclusters and made it possible to evaluate their electronic spectrum. The contribution of electron–hole pairs photoexcited in Si is observed, when the quanta energy exceeds the band gap value. In the spectral range $h\nu < 1.1$ eV, in which *c*-Si is transparent, interband indirect transitions take place via the states in the valence and conduction bands of nanoclusters. Actually, IR photoresponce in the range from 0.48 to 0.7 eV is 10–100 times lower compared to photocurrent associated with intrinsic absorption in the Si substrate. Taking into account the small volume of Ge NCs we cannot expect other behaviour. Urbach tail in PC spectra below band gap of Si (∼0.8–1.1 eB) may be caused by different kinds of uniformity in the underlying Si substrate. Moreover, this phenomenon has been observed in the previous work for structures with low density of Ge NCs [9].

Non-equilibrium carriers photoexcited in nanoclusters do not contribute into carrier transport directly. In order to contribute into the lateral current, the non-equilibrium electrons and holes should be spatially separated. As for Ge/Si heterojunctions, studied systems referred to type II, where strong confinement for holes in the region of Ge nanoclusters occurs. In the studied heterostructures, electrons can tunnel through the oxide $SiO_x$ film into the near-surface silicon region and make contribution into conductivity. At the same time, non-equilibrium holes are localized in the valence band of Ge nanoclusters; however, they can affect the potential relief in the near-surface region of Si substrate, and hence, make an indirect effect on the system conductivity. The studies of ac and dc conductivity will be presented in detail in the next paper.

Thus, photoconductivity of the structures in the range of Si transparency is unipolar—intrinsic absorption of light in nanoclusters leads to an increase of the electron concentration in the Si potential well near the $SiO_x$–Si interface and to an increase of the surface conductance. In this case, the shape of lateral photoconductivity spectra reflects the main features of intrinsic absorption of light in nanoclusters. The edge of the PC spectrum of the investigated structures at $h\nu > \varepsilon_0$ is described by the dependence typical for the indirect band semiconductors

$$\alpha(h\nu) = \frac{C}{h\nu}(h\nu - \varepsilon_0)^2, \qquad (2)$$

where $C$ is a constant, $\varepsilon_0$ is the width of the optical band gap. At excitement with quanta $h\nu < \varepsilon_0$ the Urbach tail is observed due to the crystal structure disorder [9]. Defects of crystalline structure of Ge can also give a contribution to absorption spectra and has an impact on threshold energy only and estimation of NC's band gap value. However, fundamental absorption of crystalline Ge NCs should be much greater than absorption caused by Ge defects. In order to avoid the described problem with band gap determination we plot the low-energy part of PC spectra in $(\alpha(h\nu)\cdot h\nu))^{0.5}$ versus $h\nu$ coordinates for wide spectral range.

Photocurrent spectroscopy and x-ray diffraction demonstrate that the nanoclusters have the local structure of body-centred-tetragonal Ge, exhibiting an optical adsorption edge at $\varepsilon_0$ =0.48 eV. Taking into account quantum-size effect, this is in good agreement with the theoretical calculations of electronic and optical properties of bulk body-centred-tetragonal Ge and Si, according to which the band gap width for the mentioned polytypes is 0.38 and 0.86 eV, respectively [21].

The intrinsic absorption edge for nanoclusters with silicon coverage is shifted to $\varepsilon_0 = 0.7$ eV and $\varepsilon_0 = 0.73$ eV for samples B and C, correspondingly. Increasing of optical band gap value after deposition of Si is caused by Si–Ge intermixing. Appearance of SiGe alloys is confirmed by x-ray diffraction measurements. The observed 'blue' shift is due to formation of tetragonal SiGe nanoclusters the band gap width of which is larger than that of tetragonal Ge. The adsorption of pure Ge nanoclusters was completely absent in structures with deposited silicon. Moreover, Si–Ge interdiffusion leads to decreasing of valence band offset. As a consequence, we observed a lower value of photocurrent for structure B compared to structure A due to enhanced rate of electron-hole recombination via interface states. Further increasing of deposited Si thickness to 45 MLs leads to formation of additional conductive channels through the polycrystalline Si cover layer with high concentration of defects. As a consequence, sample C shows higher photoconductivity and dark current.

It should also be mentioned that in formation of the polycrystalline silicon layer stacking faults are created mainly in the nanocluster's boundaries. It was shown experimentally and theoretically that such defects create deep levels in the band gap of silicon. In the spectra of the structures with polycrystalline diamond-like Si coverage, the component of the photocurrent can be distinguished in the range with the edge at ∼0.8 eV, which was not observed in the spectra of the structure with Ge nanoclusters. This feature can be explained by transitions via deep levels in polycrystalline Si. It is known that nanostructured silicon layers grown on the layer of germanium islands on the oxidized silicon surface are characterized by a broad photoluminescence (PL) band with a maximum at around 0.8 eV [27]. The physical reason of appearance of such a PL band is optical transitions via defect and dislocation levels in Si [28], which lead to observation at low temperature of PL bands (D1-D4) with maxima at 0.807 eV, 0.870 eV, 0.935 eV and 1.0 eV. We cannot rule out that the contribution into photoconductivity at $h\nu > 0.8$ eV is due to optical transitions via the deep defect states of the silicon coverage.

## 5. Conclusions

Germanium nanoclusters are grown by a molecular-beam epitaxy technique on a chemically oxidized Si(1 0 0) surface at 700 °C. The nanoclusters appeared to have a high density of about $3 \times 10^{11}$ $cm^{-2}$ and height about 10 nm. A possible mechanism for the initial stage of nanocluster growth is associated with creation of Si–Si bonds during vacuum annealing of $SiO_2$, which act as nucleation centres. X-ray diffraction and photocurrent spectroscopy demonstrate that the nanoclusters have the local structure of body-centred tetragonal Ge exhibiting an optical absorption edge at 0.48 eV. The usual diamond-like crystal structure of Ge nanoclusters appears to be completely absent due to isolation from Si(1 0 0) substrate. Further deposition of silicon on the surface with Ge nanoclusters leads to the surface reconstruction and formation of polycrystalline diamond-like Si coverage, while nanoclusters' core becomes tetragonal SiGe alloy. The intrinsic absorption edge for nanoclusters with silicon coverage is shifted to 0.73 eV due to Si–Ge intermixing.

## Acknowledgment

The research was supported by the program of fundamental research of the National Academy of Sciences of Ukraine 'Nanostructured systems, nanomaterials, nanotechnologies' through the Project No9/07 and by the Ministry of Education and Science of Ukraine through Project no M/34-09.

## References

[1] Brunner K 2002 *Rep. Prog. Phys.* **65** 27
[2] Schmidt O G and Eberl K 2000 *Phys. Rev.* B **61** 13721
[3] Masini G, Colace L and Assanto G 2002 *Mater. Sci. Eng.* B **89** 2
[4] Tiwari S 1995 *IEEE Int. Electron. Devices Meeting* 521–4
[5] Wu J H and Li PW 2007 *Semicond. Sci. Technol.* **22** S89
[6] Shklyaev A A and Ichikawa M 2001 *Phys. Rev.* B **65** 045307
[7] Shklyaev A A, Shibata M and Ichikawa M 2000 *Phys. Rev.* B **62** 1540
[8] Zhang L, Ye H, Huangfu Y R, Zhang C and Liu X 2009 *Appl. Surf. Sci.* **256** 768
[9] Lysenko V S, Gomeniuk Y V, Kozyrev Y N, Rubezhanska M Y, Sklyar V K, Kondratenko S V, Melnichuk Y Y and Teichert C 2011 *Adv. Mater. Res.* **276** 179
[10] Nakamura Y, Ichikawa M, Watanabe K and Hatsugai Y 2007 *Appl. Phys. Lett.* **90** 153104
[11] Chen Y, Lu Y F, Tang L J, Wu Y H, Cho B J, Xu X J, Dong J R and Song W D 2005 *J. Appl. Phys.* **97** 014913
[12] Baribeau J-M, Wu X, Rowell N L and Lockwood D J 2006 *J. Phys.: Condens. Matter.* **18** R139
[13] Kasper E, Schuh A, Bauer G, Holländer B and Kibbel H 1995 *J. Cryst. Growth* **157** 68
[14] Lysenko V S, Gomeniuk Y V, Strelchuk V V, Nikolenko A S, Kondratenko S V, Kozyrev Y N, Rubezhanska MY and Teichert C 2011 *Phys. Rev.* B **84** 115425
[15] Tromp R, Rubloff G W, Balk P, LeGoues F K and van Loenen E J 1985 *Phys. Rev. Lett.* **55** 2332–5
[16] Skorupa W, Rebohle L and Gebel T 2003 *Appl. Phys.* A **76** 1049
[17] Shklyaev A A and Ichikawa M 2008 *Phys.- Usp.* **51** 133
[18] Barski A, Derivaz M, Rouvière J L and Buttard D 2000 *Appl. Phys. Lett.* **77** 3541
[19] Shklyaev A A, Shibata M and Ichikawa M 2000 *Rev.* B **62** 1540
[20] Leonhardt D, Ghosh S and Han S M 2011 *J. Appl. Phys.* **110** 073516
[21] Malone B D, Louie S G and Cohen M L 2010 *Phys. Rev.* B **81** 115201
[22] Fujimoto Y, Koretsune T, Saito S, Miyake Y and Oshiyama A 2008 *New J. Phys.* **10** 083001
[23] Kanemitsu Y, Uto H, Masumoto Y and Maeda Y 1992 *Appl. Phys. Lett.* **61** 2187
[24] Saito Y 1979 *J. Cryst. Growth* **47** 61
[25] Jiang J, Chen K, Huang X, Li Z and Feng D 1994 *Appl. Phys. Lett.* **65** 1799
[26] Jamieson J C 1963 *Science* **139** 762
[27] Shklyaev A A and Ichikawa M *Appl. Phys. Lett.* **80** 1432
[28] Drozdov N A, Patrin A A and Tkachev V D 1976 *JETP Lett.* **23** 597